RAPID COMMUNICATIONS IN MASS SPECTROMETRY
Rapid Commun. Mass Spectrom. 2008; **22**: 1062–1068
Published online in Wiley InterScience (www.interscience.wiley.com) DOI: 10.1002/rcm.3469

RCM

Ion internal energy distributions validate the charge residue model for small molecule ion formation by spray methods

David Touboul†, Matthias Conradin Jecklin† and Renato Zenobi*
Department of Chemistry and Applied Biosciences, ETH Zürich, CH-8093 Zürich, Switzerland

Received 12 November 2007; Revised 28 January 2008; Accepted 28 January 2008

This paper reports a detailed study of the internal energy distribution of ions formed by four electrospray ionization (ESI)-related ionization methods, with particular emphasis on electrosonic spray ionization (ESSI). Substituted benzylpyridinium ions were used as thermometer ions to probe the internal energy distribution. The influence of different instrumental parameters was studied. Cone and skimmer voltages as well as the collision energy were found to strongly affect the ion internal energy distribution, whereas the distance between the emitter and the inlet of the mass spectrometer, the nebulizing gas pressure or the flow rate showed no influence. The internal energy distribution obtained with an ESSI source was compared with those obtained for electrospray (ESI), nanoelectrospray (nanoESI) and sonic spray ionization (SSI) on the same mass spectrometer with the same instrumental parameters. No clear differences were observed. As the charge residue model is the only ion formation mechanism possible for SSI, we conclude that benzylpyridinium ions are formed by the pathway suggested by this model. Copyright © 2008 John Wiley & Sons, Ltd.

Non-covalent interactions between biomolecules play key roles in life. Numerous analytical techniques have been developed in order to access to the specificity and the strength of these solution-phase interactions.[1] Mass spectrometry, and especially electrospray ionization (ESI),[2] is an efficient tool to study non-covalent interactions between various species (protein-protein, protein-small molecules, protein-DNA, DNA-DNA . . .),[3–8] and the data can be related to solution-phase structures when controlled conditions are used. ESI can be operated as a very soft ionization technique, i.e. the internal energy distribution of the produced ions is low compared with, for example, particle bombardment (secondary ion mass spectrometry or fast atom bombardment).[9] Nevertheless, the energy transferred to a complex during the ionization/desolvation processes in ESI can be sufficient to dissociate the non-covalently bound species present in solution. Therefore, the ion source and the mass spectrometer parameters must be tuned very carefully to observe non-covalent complexes by mass spectrometry.

Sonic spray ionization (SSI) is a technique developed by Hirabayashi *et al*. in the 1990s,[10,11] and it has recently become commercially available as a liquid chromatography/mass spectrometry (LC/MS) interface. SSI uses a nitrogen gas flow at sonic speed coaxial to a fused-silica capillary. This provides efficient pneumatic spraying of the nebulizing gas under electrically neutral conditions, i.e. there is no voltage applied to the capillary. At a spray distance of 5 mm the ion signal intensity strongly depends on the gas velocity and reaches a maximum at sonic gas speed (Mach number ≈1). The intensities of ions generated by ESI and SSI show differences, probably because no electric field is applied to the capillary for SSI, leading to different pathways for charged-droplet formation. It was also shown that the charged-droplet formation for SSI can be ascribed to the statistical charging model proposed by Dodd,[12] which is also generally accepted as the mechanism for thermospray. Presumably due to the low internal energy of the ions, excessive clustering often occurs in SSI, which can adversely affect the analytical performance of the method for molecular characterization. To date, SSI has been successfully applied to the analysis of a number of compounds in environmental and biological samples.[13–16]

ElectroSonic Spray Ionization Mass Spectrometry (ESSI-MS)[17,18] was developed by Cooks' group in 2004. This technique uses an SSI source, but includes a high voltage applied to the capillary, leading to a narrow charge-state distribution. This narrow charge-state distribution is probably due to the production of ions that are either completely desolvated or nearly so before they enter the mass spectrometer. A travel time of a few hundreds of microseconds for ions between the spray tip and the entrance of the mass spectrometer inlet was estimated to correspond to a linear velocity of the nebulizing gas of 350 $m \cdot s^{-1}$. It has been demonstrated that non-covalent complexes can be kept intact in the gas phase using ESSI-MS. We have found that dissociation constants (K_Ds) derived from ESSI yielded

**Correspondence to*: R. Zenobi, Department of Chemistry and Applied Biosciences, ETH Zürich, CH-8093 Zürich, Switzerland.
E-mail: zenobi@org.chem.ethz.ch
†These authors contributed equally to this work.
Contract/grant sponsor: Novartis Institutes for BioMedical Research.

values lower than those measured by ESI and nanoESI, and closer to solution-phase data, which is evidence for the softness of this method.[19]

The greater softness of SSI or ESSI than of ESI or nanoESI is only supported by few examples in the literature, and for specific cases.[10,11,17–19] We therefore decided to compare the internal distribution energy of these four different techniques on the same instrument under the same instrumental settings, using so-called 'thermometer' ions with the 'survival yield method'.[9,20–23] Our goal was to show whether it is the ion internal energy that determines the softness of SSI and ESSI, or whether other aspects need to be taken into account. Moreover, the influence of a number of instrumental parameters (spray distance and angle, voltage, gas pressure, flow rate, cone voltage and temperature) on the internal energy distribution in ESSI was investigated.

EXPERIMENTAL

Materials and sample preparation

Benzylpyridinium salts were kindly provided by V. Gabélica and E. De Pauw (University of Liège). A stock solution of $1\,mg \cdot mL^{-1}$, containing an equimolar mixture of six benzylpyridinium salts (Table 1), was prepared in water and then diluted 100-fold with water/methanol (50:50). Only *para*-substituted benzylpyridiniums were used because all precursor and fragment ions have different masses and can be injected at the same time. Moreover, compared with *ortho*- and *meta*-substituted salts, their calculated dissociation energy barrier, also called critical energy, E_0, covers the largest range.

Mass spectrometry

Mass spectrometric analysis was performed with a hybrid quadrupole time-of-flight mass spectrometer (Q-Tof Ultima; Waters/Micromass Ltd., Manchester, UK) equipped with a Z-spray interface. The instrument was controlled via the Waters MassLynx software (version 4.0). All measurements were performed in positive ion mode. The source temperature was kept at 40°C, the cone voltage was kept at 50 V, the RF lens1 voltage – the potential applied to the first ion tunnel (hexapole) in the linear flight path, which plays the same role as a skimmer (in linear interface instruments) – was kept at 50 V. Argon was used as collision gas and a typical setting of 10 eV was used for the collision energy parameter for optimized sensitivity. The transmission of the ions was optimized on the quadrupole for the required mass range (m/z 100–300). Mass spectra were accumulated for 2–3 min to obtain a good signal-to-noise ratio. Mass calibration of the instrument was performed using the sodium iodide (NaI) clusters generated by spraying a solution of NaI in water/2-propanol (1:1, v/v) at a concentration of $2\,\mu L.min^{-1}$.

Table 1. The *para*-substituted benzylpyridium ions used for the internal energy distribution are given in the first column. Columns two and three show the observed m/z of precursor and fragment ions used to calculate the SY. The degrees of freedom (DOF) and the fragmentation critical energies (E_0)[24] of the ions are given in the last two columns

R	$m/z_{precursor}$	$m/z_{fragment}$	DOF	E_0 (eV)
p-OCH_3	200	121	81	1.51
p-F	188	109	69	1.87
p-Cl	204/206	125/127	69	1.9
p-CN	195	116	72	2.1
p-NO_2	215	136	75	2.35

ESI measurements were performed using the manufacturer's standard ESI source (Waters/Micromass Ltd.). The i.d. of the spray capillary was 75 μm and the spray distance was around 1 cm.

The SSI/ESSI source – with some modifications as described by Jecklin *et al*.[19] – was home-built following the design described by Takáts *et al*.[17] For SSI, the same set-up was used but no voltage was applied to the capillary. The high voltage (0–3 kV) was connected to a stainless steel union (Upchurch Scientific Inc., Oak Harbor, WA, USA). The SSI/ESSI source was mounted on an *x*-*y*-*z*-positioning stage. A spray distance of between 1 and 30 cm was used and three different spray angles (0°, 45° and 90°) were tested for ESSI. Nitrogen was used for the sonic nebulizing gas at a pressure between 4 and 22 bar, which led to a gas flow rate of 5–20 $L.min^{-1}$ on the spray tip. A model 22 syringe pump (Harvard Apparatus GmbH, March-Hugstetten, Germany; 5–10 $\mu L \cdot min^{-1}$ flow rate) was used for sample infusion using ESI, ESSI and SSI.

NanoESI measurements were performed using an automated chip-based nanoESI robot (NanoMate model 100; Advion Bioscience, Ithaca, NY, USA). This holds a 96-well sample plate, a rack of 96 disposable, conductive pipet tips and a nanospray chip containing 20×20 nozzles of 5 μm diameter each. A gentle backing pressure of 4–6 bar on the spray tip was used to assist the liquid sample flow.

To evaluate the sensitivity versus the spray distance for ESSI, a spectrum at each distance was recorded for 30 s, after the spray had stabilized. The signal intensity of the ion at m/z 204, corresponding to the precursor ion of the *para*-chlorobenzylpyridinium ion, was then plotted against the distance. The reproducibility was tested using four different acquisitions with exactly the same parameters and the same capillary, leading to an estimated standard deviation of ~2%.

RESULTS AND DISCUSSION

Determination of internal energy distribution

The survival yield method is based on two major assumptions: (i) all precursor ions having similar structures and number of degrees of freedom will have the same internal energy distribution; (ii) all precursor ions having an internal energy higher than the dissociation energy barrier (E_0), also called critical energy, will dissociate, whereas those having an internal energy lower than E_0 will stay intact. Under these considerations, the molecular survival yield (SY) can be defined as:

$$SY = \frac{I_{P^+}}{I_{P^+} + I_{F^+}}$$

where I_P^+ is the intensity of the precursor ion signal and I_F^+ is the intensity of the fragment ion signal. It represents the fraction of precursor ions that have an internal energy below the dissociation threshold E_0. The SY obtained for each precursor ion is then plotted as a function of the critical

DOI: 10.1002/rcm

RCM

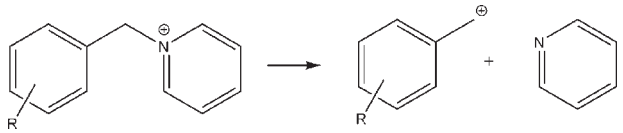

Figure 1. Dissociation reaction of benzylpyridium cations.

energy E_0. Two data points ($E_0 = 0$ eV; SY = 0 and $E_0 = 4$ eV; SY = 1) are added, because no precursor ions remain if the critical energy is equal to zero and no fragmentation occurs when the critical energy is high (4 eV). As demonstrated in the review of Gabélica and De Pauw,[9] the internal energy distribution can be obtained by the derivative dSY(E)/dE. For evaluating our experiments, we chose a simple procedure to obtain the mean internal energy value: we first fitted the SY(E) curve by a sigmoidal curve and then derived this fitted curve. This approximation is valid because the internal energy distribution always shows an overall Gaussian-like shape.

Benzylpyridinium ions have been introduced as 'thermometer' ions by De Pauw's group.[20–23] Benzylpyridinium ions are the perfect choice for the survival yield method, because all the precursor ions have similar sizes and degrees of freedom and are characterized by the similar internal energy distribution. This family of compounds fragments by a well-known pathway, a simple cleavage of the C–N bond between the substituted benzyl radical and the pyridine, leading to the formation of a substituted benzyl cation and a pyridine (Fig. 1). This specific dissociation is characterized by a loose transition state, meaning that there is no activation barrier for this fragmentation pathway. Each critical energy (E_0) can be easily calculated as the difference between the heats of formation of the products and the reactant. Different values for E_0 have already been published and depend mainly on the level of calculation (semi-empirical, *ab initio* or DFT). The values published by Gabélica *et al*. have been chosen (Table 1) because the semi-empirical Austin Method 1 (AM1) gave critical energy values that agree well with experimental survival yields.[24] In our work, no kinetic shift correction was introduced in the calculation. This approximation is still acceptable because we only compare between different ion sources, using exactly the same instrumental parameters; no quantitative measurement of the mean internal energy was sought.[9] An example of the different steps needed to determine the mean internal energy from experimental data points is shown in Fig. 2. While data from different benzylpyridinium ions are necessary to obtain mean internal energy values, data from a single benzylpyridinium ion are sufficient to survey the effects of experimental parameters on the internal energy distribution because all the benzylpyridinium ions have exactly the same internal energy.[24]

Influence of the cone and skimmer (RF lens1) voltages and of the collision energy on the internal energy distribution of ions produced by ESI, nanoESI and ESSI

Figures 3(a) and 3(b) show the influence of the cone voltage and RF lens1 (skimmer) voltage on the SY of the *para*-chlorobenzylpyridinium ions formed by ESI, nanoESI and ESSI. *para*-Chlorobenzylpyridinium was chosen because it showed the largest influence of the experimental parameters on the internal energy when comparing the three ionization methods. For the other thermometer ions, the trend was identical but less pronounced. When 50 V was applied to RF lens1, and for cone voltages lower than 90 V, the SY is stable and close to 100% for all ionization techniques. For higher values of the cone voltage, a decrease in the SY is observed for all ion sources. When 45 V was applied to the cone, and for RF lens1 voltages lower than 70 V, the SY is stable and equal to ~0.98 for all techniques. For higher values of the RF lens1 voltage, the SY decreases for all ion sources. However, in both cases, this trend is more pronounced for ESI and nanoESI than for ESSI.

As described extensively by Gabélica and De Pauw,[9] the internal energy distribution mainly depends on the supersonic expansion at the cone level, and on the ion optics (geometry and voltage applied) of the first stage of the mass

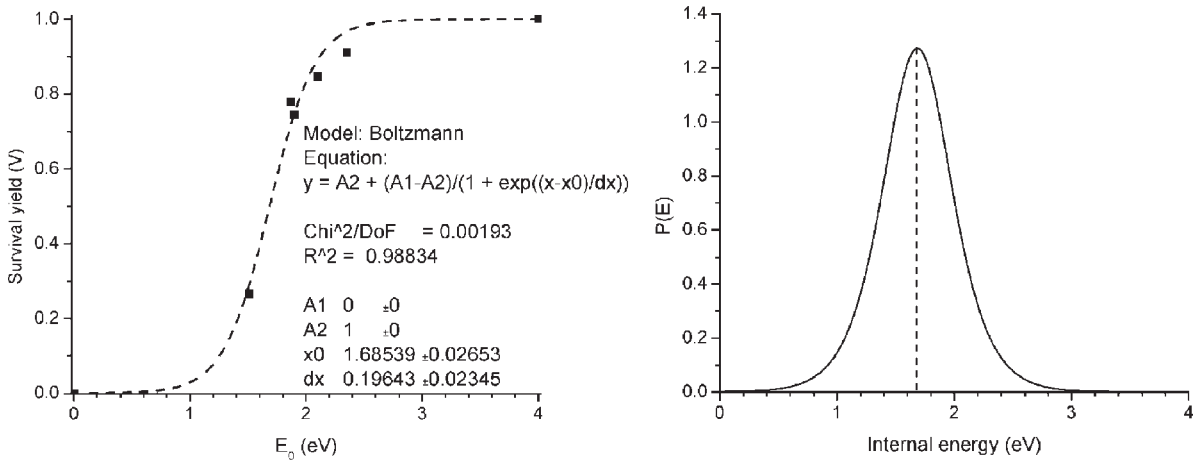

Figure 2. (A) The survival yields of the *para*-substituted benzylpyridium ions are plotted as a function of their calculated fragmentation critical energies. Two points (0,0) and (4,1) were added manually, the dotted line shows the sigmoid fit of the points. The parameter X0 fitted by a Boltzmann distribution corresponds to the mean internal energy. (B) Internal energy distribution of the *para*-substituted benzylpyridium ions determined by the derivation of the sigmoid fit shown in (A).

DOI: 10.1002/rcm

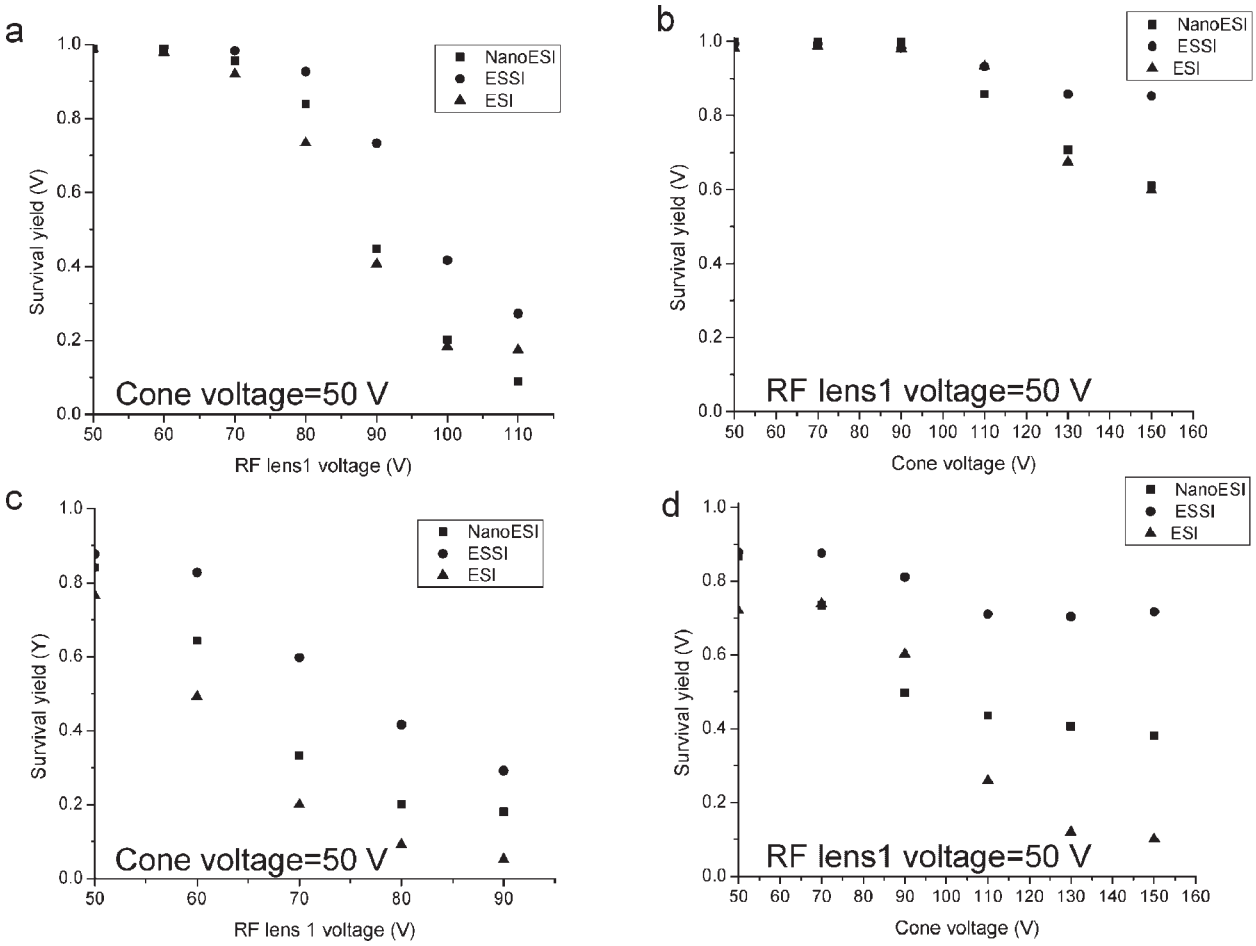

Figure 3. Comparison of three different ionization techniques (ESI, nanoESI and ESSI) and the influence of instrumental parameters on the survival yield (SY) of *para*-substituted benzylpyridium ions. (A, B) Breakdown curves of the *para*-chlorobenzylpyridinium ion ($E_0 = 1.90$ eV) with increasing voltage on the RF lens1 (cone voltage kept at 50 V) and the sampling cone (RF lens1 kept at 50 V), respectively. (C, D) Breakdown curves of the *para*-methoxybenzylpyridinium ions ($E_0 = 1.51$ eV).

spectrometer where an intermediate pressure is applied. The supersonic expansion, due to the pressure difference, induces a cooling of the analytes (a decrease in their internal energy).[25] Subsequently, charged droplets and/or ions are accelerated by the potentials on the cone (and on the skimmer in a linear interface). In our experiments using a Q-Tof with Z-shaped interface, the RF lens1 plays the same role as the so-called skimmer in other sources. The ions accelerated in the RF lens1 undergo collisions with the residual neutral gas which causes desolvation of the droplets, ion cooling at lower RF lens1 voltages but also ion activation and dissociation at higher voltages. Increasing the RF lens1 voltage will lead to more energetic collisions with the neutral gas and to an increase of the internal energy. This explains the observed decrease of the SY when increasing the cone or RF lens1 voltage, as described previously for ESI.[23]

The balance between cooling by supersonic expansion and excitation after acceleration by the different voltages explains the differences observed at high cone or RF lens1 values for the different ionization techniques. It is also well known that droplets formed by ESI or nanoESI have a velocity around $5\,m \cdot s^{-1}$,[26] measured close to the Taylor cone, whereas droplets formed by ESSI have the same velocity as the nebulizing gas, around $350\,m \cdot s^{-1}$ at the very end of the spray tip.[17] Moreover, ESSI has been reported to produce much finer initial droplets than ESI.[17] Therefore, we can assume that the droplets formed by ESSI will be desolvated in a shorter time than the ones formed by ESI or nanoESI, due to their smaller initial size and/or their higher velocitiy, i.e. higher number and greater efficiency of collisions between the charged droplets and the ambient gas. Thus, ESSI should form colder ions than ESI or nanoESI. At low values of the cone or skimmer voltages, the SY of the *para*-chlorobenzylpyridinium ions is close to 1 in all cases, implying that the ion cooling is sufficient and dissociation of the compounds is prevented for all techniques. For higher values, the ion activation by collisions will be enough to observe the fragmentation on the time scale of the experiment. As the ions formed by ESSI should be colder, the threshold to detect a certain amount of fragmentation should be higher than for ESI and nanoESI, which was indeed observed experimentally. This was confirmed by studying the effects of the RF lens1 (Fig. 3(c)) or cone voltage (Fig. 3(d)) on the fragmentation of the *para*-methoxybenzylpyridinium ion, which shows a lower critical energy ($E_0 = 1.51$ eV) than the *para*-chlorobenzylpyridinium ion ($E_0 = 1.90$ eV). For the lowest value of the RF lens1 voltage, the SY is the highest for ESSI (~0.9), followed by nanoESI (~0.85) and ESI (~0.77).

DOI: 10.1002/rcm

RCM

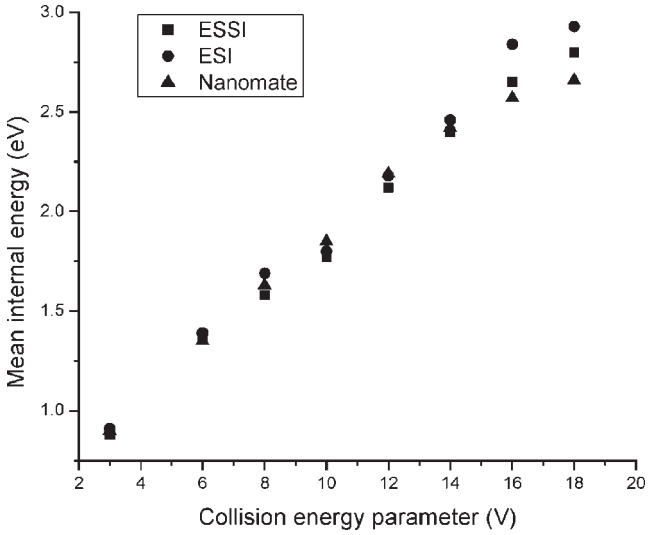

Figure 4. The influence of the collision energy setting on the mean internal energy (of all ions) for the investigated three ionization techniques, ESI, nanoESI, and ESSI.

Thus, the initial droplet size and the time needed for a complete desolvation play key roles in determining the ion internal energy distribution. These observations on small molecules are also confirmed by the fact that a higher RF lens1 voltage is needed to destroy a complex between lysozyme and a sugar (*N*,*N*′,*N*′′- triacetylchitotriose) formed by ESSI, than by ESI or nanoESI.[19]

The influence of the collision energy on the internal energy of the ions is shown in Fig. 4. As expected, the internal energy increases linearly with increasing collision energy. The maximum center-of-mass energy (E_{CM}) that an ion can receive during a collision with a neutral is equal to:

$$E_{CM} = E_{lab} \times \frac{M_{gas}}{M_{ion} + M_{gas}}$$

where E_{lab} is the laboratory-frame kinetic energy of the ion, M_{gas} the mass of the neutral gas, and M_{ion} the mass of the ion. Part of E_{CM} will be converted into kinetic energy, and the rest will be converted into internal energy. It must be noted that by increasing E_{lab}, the mean internal energy of the ion will increase approximately linearly and this effect is independent of the ion source. When increasing the E_{lab} by 10 eV, the E_{CM} is increased by ~1.67 eV. Experimentally, an internal energy increase of about 1.3 eV is observed when the E_{lab} is increased by 10 eV.

Influence of source parameters on the internal energy distribution of ions produced by ESSI

The intrinsic parameters of the ESSI source (distance, angle, pressure of the nebulizing gas and flow rate) were also studied. The influence of the voltage applied will be discussed in the next section. The influence of the angle (0, 45 and 90°) between the spray tip and the cone at the entrance of the mass spectrometer was explored for different distances (1–30 cm). For an angle of 0°, corresponding to a perfect alignment between the spray and the symmetry axis of the cone, the mean internal energy first increases by 2% between 1 and 2 cm, reaches 1.71 eV for a distance between 2 and 6 cm and then decreases to 1.68 eV for distances ≥10 cm (Fig. 5(a)). The estimated measurement uncertainty is 2%, i.e. the variation of the mean internal energy as a function of distance is negligible. Similar observations were made when varying the angle at a given distance, the distance for different angles, the flow rate of the sample (Fig. 5(b)) or the pressure of the nebulizing gas (Fig. 5(c)).

Our results confirm that the intrinsic parameters of the ion source (distance, angle, flow rate, pressure of the nebulizing gas) play a minor role in determining the ion internal energy for ESSI. The main ion activation occurs by collisions at the level of the cone and the skimmer and directly depends on the voltages applied on the different ion optical elements. By increasing these voltages, the ion kinetic energy increases, leading to a higher collision rate with the drying gas and a higher internal energy.

For all angles and all nebulizing gas pressures in the range 5–20 bar, at the same flow rate of the sample, the best sensitivity (Fig. 6) was achieved for distances around 6 cm. The sensitivity decreases when the distance between the spray tip and the cone is too short or too long (<4 cm or >10 cm). For short distances, below 4 cm, solvent molecules in the spray gas are cooled by adiabatic expansion leading to formation of clusters. This phenomenon greatly reduces the sensitivity for ion detection.[10,11] This is confirmed by the fact that the sensitivity does not increase when increasing the liquid flow rate of the sample to more than 10 μL min^{-1}. Due to the spray divergence and a higher deceleration of the droplets by collisions with the ambient air at atmospheric pressure, the sampling efficiency at the level of the cone decreases when the distance is too long (>10 cm). Takáts *et al*. have shown that peak broadening occurred for lysozyme when the distance was too short, due to re-solvation in the first stage of the mass spectrometer.[17] The best full width at half maximum values are obtained for distances longer than 10 cm, which is the best compromise between good desolvation and sensitivity. All these experiments suggest that the same effects are observed for small ions, like the benzylpyridinium ions, or large ions, like protein ions.

Ion evaporation or charge residue model?

The mechanism of ion generation using ESI is still a highly debated question.[27,28] The ion evaporation model (IEM) states that at a certain point below the Rayleigh limit, i.e. for a droplet radius below 10–20 nm, the electric field on the surface of the charged droplets is sufficiently high that solvated ions are emitted directly into the gas phase.[29–31] In the charge evaporation model (CRM), Dole and coworkers stated that successive Coulomb fissions will lead to the formation of nanodroplets containing only a single analyte molecule if the concentration of the analyte is low enough.[32] The analyte surrounded by some solvent molecules will retain the charge state of the nanodroplet and a gas-phase ion will be formed after desolvation, which mainly takes place in the interface of the mass spectrometer. There is some evidence that the IEM applies to small ions, like sodium clusters,[33–35] whereas the CRM more accurately describes the situation for large ions, such as those from peptides and

DOI: 10.1002/rcm

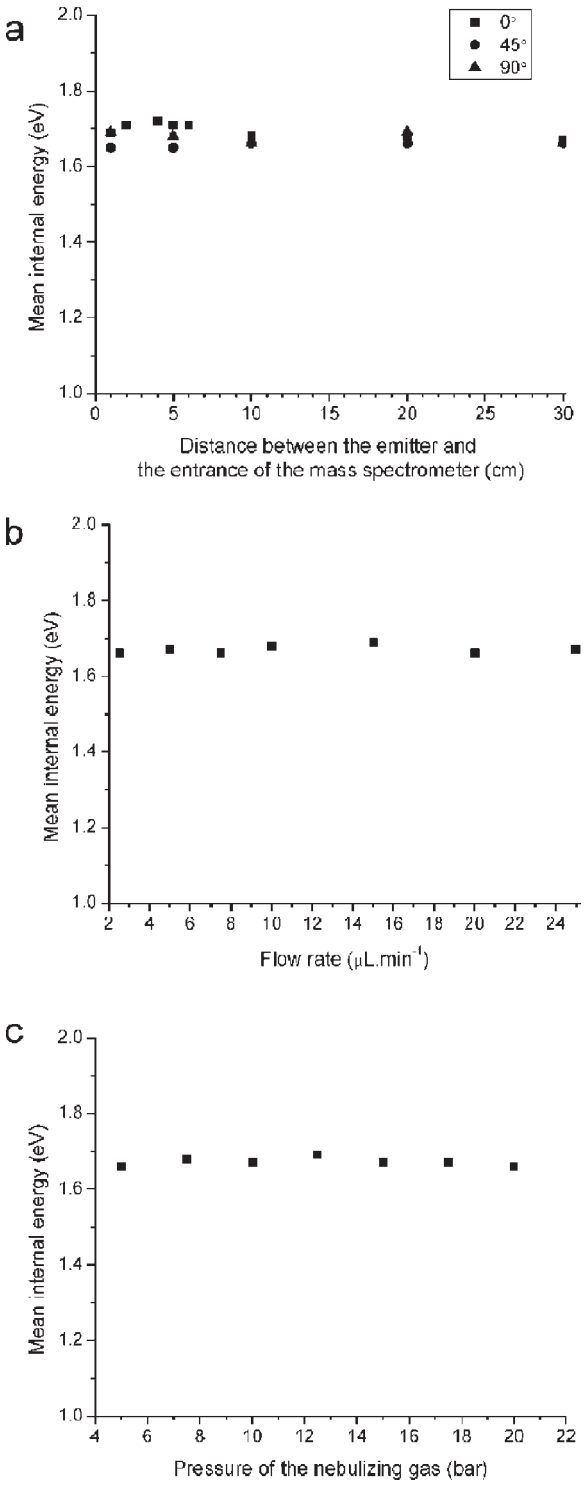

Figure 5. Study of the intrinsic parameters of ESSI and their influence on the internal energy distribution of *para*-substituted benzylpyridium ions. (A) Mean internal energy as a function of three different spray angles (linear to the sampling cone (0°), in a 45° and 90° angle to the sampling cone) and the dependence on the spray distance. Influence of (B) the flow rate and (C) the nebulizing gas pressure.

proteins.[27,36] Nevertheless, the distinction between 'small' and 'large' ions is unclear. One can also ask which ion formation model would best describe the case of the benzylpyridinium ions, small organic ions that are already charged in solution.

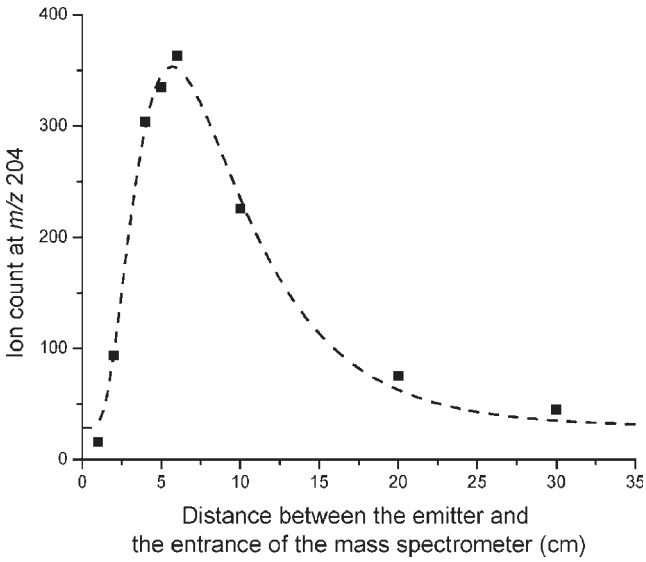

Figure 6. The sensitivity (ion count for the precursor *para*-chlorobenzylpyridinium ion) determined as a function of the spray distance.

In the IEM, the Coulomb repulsion between the charged ion and the charged droplet induces an increase in kinetic energy of the ion, which is partially converted into internal energy by collision with the bath gas. Takáts *et al*. estimated that the kinetic energy transferred to an ion is ~20–30 eV and 5–15% of this, i.e. ~1–4 eV, is converted into internal energy.[37] Thus, the ions formed according to the IEM should have a significantly higher internal energy than the ones formed according to the CRM.

The charged-droplet formation in SSI is based on the statistical charging model;[38] thus the gaseous ion formation must be based on the CRM.[39] The 'statistical charging model' means that the bulk liquid is quickly evaporated forming small droplets with more or less the same diameter. Most of the droplets are neutral because the same numbers of negatively and positively charged ions are present. Nevertheless, microscopic fluctuations in the ion concentration in the bulk liquid lead to the formation of some positively or negatively charged droplets. According to this model, the average charge of the droplet <q> is proportional to the square root of the ion concentration in solution. Takáts *et al*. showed for SSI that with the addition of strong electrolytes (i.e. NaCl) the signal intensity of amino acid cluster ions increased linearly with the electrolyte concentration over the range of 0–1 mM.[13] Moreover, the Rayleigh limit is not likely to be reached, and shrinking of the droplet until complete evaporation is supposed to occur. This mechanism corresponds to the CRM. If the difference in ion internal energy is linked to differences in the ion production mechanism, then the ion energy distribution measurement could be a probe for the ion formation mechanism. Thus, the ion energy distribution was also measured for SSI and compared with that for ESSI, ESI and nanoESI (Fig. 7), with exactly the same parameters for the mass spectrometer interface, meaning the same cone (45 V), RF lens1 (50 V) and collision energy (10 eV) values.

DOI: 10.1002/rcm

RCM

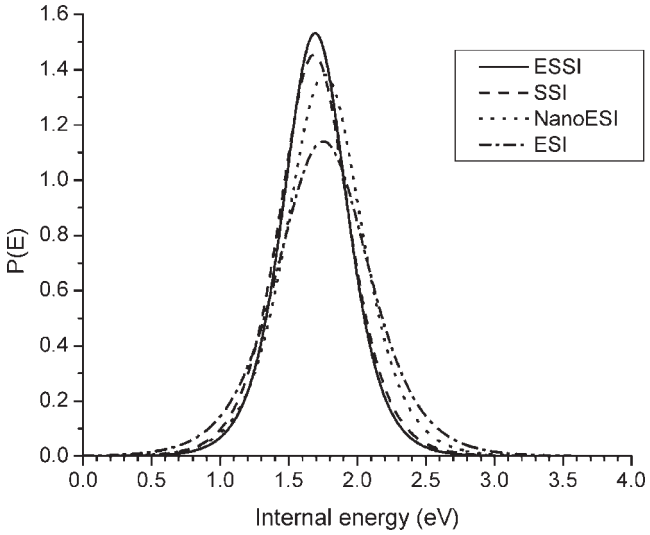

Figure 7. The internal energy distribution of *para*-substituted benzylpyridium ions compared for different ionization techniques (ESI, nanoESI, ESSI and SSI), while keeping all instrumental parameters strictly constant. The curves are all very similar (within an experimental error of 2%), indicating that the ion formation mechanism must be the same for all spray techniques.

Figure 7 shows a slight shift to higher mean internal energy and broader distribution when going from ESSI, to SSI, to nanoESI, to normal ESI. Nevertheless, all these curves are very close to each other, implying that the ion formation mechanism must be the same, i.e. the charge residue model (CRM). The only real difference between all these ion sources is the speed of desolvation. It is this rapid desolvation that leads to colder ions and a softer ionization process for ESSI and SSI than for ESI and nanoESI.

CONCLUSIONS AND OUTLOOK

We have demonstrated that only the cone and the RF lens1 voltages (corresponding to skimmer voltages of linear spray interface instruments) and the collision energy have a significant effect on the internal energy distribution of ions formed by ESSI. ESSI leads to colder ions than ESI and nanoESI, especially when high values of the cone or skimmer voltages are used. Moreover, we found that all benzylpyridinium ions examined are produced in the gas phase according to the charge residue model (CRM), for all ionization techniques investigated. We have previously published data showing that non-covalent complexes seem to be more stable when sprayed by ESSI, than by ESI and nanoESI.[19] Here, we show that the internal energy measured for ESSI, ESI and nanoESI is very close. Thus, the increase in stability of the non-covalent species sprayed by ESSI cannot be explained by a decrease in the internal energy but must be due to other effects, such as the initial droplet size, or the energy required for complete desolvation. The next improvement for ESSI will be to miniaturize this ion source in order to reach the capabilities of nanoESI in terms of spray stability, sample consumption and automation.

Acknowledgements

We thank the Novartis Institutes for BioMedical Research for financial support. We are grateful to Professor Edwin De Pauw and Valérie Gabélica for the gift of the benzylpyridinium salts.

REFERENCES

1. Hensley P. *Structure* 1996; **4**: 367.
2. Fenn JB, Mann M, Meng CK, Wong SF, Whitehouse CM. *Science* 1989; **246**: 64.
3. Ganem B, Li YT, Henion JD. *J. Am. Chem. Soc.* 1991; **113**: 7818.
4. Loo JA. *Mass Spectrom. Rev.* 1997; **16**: 1.
5. Wang WJ, Kitova EN, Klassen JS. *Meth. Enzymol.* 2003; **362**: 376.
6. Daniel JM, McCombie G, Wendt S, Zenobi R. *J. Am. Soc. Mass Spectrom.* 2003; **14**: 442.
7. Gabélica V, Galic N, Rosu F, Houssier C, De Pauw E. *J. Mass Spectrom.* 2003; **38**: 491.
8. Ashcroft AE. *Nat. Product Rep.* 2005; **22**: 452.
9. Gabélica V, De Pauw E. *Mass Spectrom. Rev.* 2005; **24**: 566.
10. Hirabayashi A, Sakairi M, Koizumi H. *Anal. Chem.* 1994; **66**: 4557.
11. Hirabayashi A, Sakairi M, Koizumi H. *Anal. Chem.* 1995; **67**: 2878.
12. Dodd EE. *J. App. Phys.* 1953; **24**: 73.
13. Takáts Z, Nanita SC, Cooks RG, Schlosser G. *Anal. Chem.* 2003; **75**: 1514.
14. Benijts T, Gunther W, Lambert W, De Leenheer A. *Rapid Commun. Mass Spectrom.* 2003; **17**: 1866.
15. Arinobu T, Hattori H, Seno H, Ishii A, Suzuki O. *J. Am. Soc. Mass. Spectrom.* 2002; **13**: 204.
16. Huang M, Hirabayashi A. *Anal. Sci.* 2002; **18**: 385.
17. Takáts Z, Wiseman JM, Gologan B, Cooks RG. *Anal. Chem.* 2004; **76**: 4050.
18. Wiseman JM, Takats Z, Gologan B, Davisson VJ, Cooks RG. *Angew. Chem. Int. Ed. Engl.* 2005; **44**: 913.
19. Jecklin MC, Touboul D, Bovet C, Zenobi R. *J. Am. Soc. Mass. Spectrom.* 2008; in revision.
20. De Pauw E, Pelzer G, Marien J, Natalis P. *Org. Mass Spectrom.* 1990; **25**: 103.
21. Derwa F, De Pauw E, Natalis P. *Org. Mass Spectrom.* 1991; **26**: 117.
22. Collette C, Drahos L, De Pauw E, Vekey K. *Rapid Commun. Mass Spectrom.* 1998; **12**: 1673.
23. Collette C, De Pauw E. *Rapid Commun. Mass Spectrom.* 1998; **12**: 165.
24. Gabélica V, Schulz E, Karas M. *J. Mass Spectrom.* 2004; **39**: 579.
25. Hayes JM, Small GJ. *Anal. Chem.* 1983; **55**: 565A.
26. Wortmann A, Kistler-Momotova A, Zenobi R, Heine MC, Wilhelm O, Pratsinis SE. *J. Am. Soc. Mass Spectrom.* 2007; **18**: 385.
27. Cole RB. *J. Mass Spectrom.* 2000; **35**: 763.
28. Nguyen S, Fenn JB. *Proc. Natl. Acad. Sci. USA* 2007; **104**: 1111.
29. Iribarne JV, Thomson BA. *J. Chem. Phys.* 1976; **64**: 2287.
30. Thomson BA, Iribarne JV. *J. Chem. Phys.* 1979; **71**: 4451.
31. Iribarne JV, Dziedzic PJ, Thomson BA. *Int. J. Mass Spectrom. Ion Phys.* 1983; **50**: 331.
32. Dole M, Mack LL, Hines RL. *J. Chem. Phys.* 1968; **49**: 2240.
33. Kebarle P, Tang L. *Anal. Chem.* 1993; **65**: 972A.
34. Wang G, Cole RB. *Anal. Chim. Acta* 2000; **406**: 53.
35. Gamero-Castano M, Fernandez de la Mora J. *J. Mass Spectrom.* 2000; **35**: 790.
36. Gamero-Castano M, Fernandez de la Mora J. *Anal. Chim. Acta* 2000; **406**: 67.
37. Takáts Z, Drahos L, Schlosser G, Vékey K. *Anal. Chem.* 2002; **74**: 6427.
38. Dodd EE. *J. Appl. Phys.* 1953; **24**: 73.
39. Deguchi K, Takegawa Y, Hirabayashi A, Nakagawa H, Nishimura S. *Rapid Commun. Mass Spectrom.* 2005; **19**: 2325.

DOI: 10.1002/rcm